PERGAMON

International Journal of Multiphase Flow 26 (2000) 949–975

International Journal of Multiphase Flow

www.elsevier.com/locate/ijmulflow

Results from a two-dimensional turbulent diffusion-model for dispersion and deposition of droplets in horizontal annular dispersed gas/liquid flow

B. Mols*, I. Mittendorff, R.V.A. Oliemans

Laboratory for Aero- and Hydrodynamics, Delft University of Technology, Delft, The Netherlands

Received 20 April 1998; received in revised form 11 July 1999

Abstract

A previously used one-dimensional Turbulent Diffusion-model is extended to two dimensions. A quasi-stationary annular dispersed gas/liquid flow is simulated by adding the contributions for different particle sizes of a large number of annular line sources from roll wave tops in the upstream direction. One or more local maxima in the droplet concentration are predicted, if droplet sources are present all along the tube wall. A local maximum in the concentration has been found in experiments as well, but it was always solely attributed to the presence of a secondary gas flow. The droplet deposition flux as calculated in the two-dimensional model shows good agreement with a previously derived analytical expression for the droplet deposition flux. Finally we derive how the two-dimensional deposition flux depends on the Stokes- and Froude-numbers. For an arbitrary Froude-number it is predicted droplets up to which Stokes-number are able to deposit at the top of the tube.

Keywords: Particle deposition; Particle dispersion; Deposition rate; Turbulent diffusion; Annular flow; Horizontal flow

1. Introduction

The present paper is an extension of the work of Binder and Hanratty (1992) and Mols and Oliemans (1998) on dispersion and deposition of droplets in horizontal annular flow. The

* Corresponding author.

0301-9322/00/$ - see front matter
PII: S0301-9322(99)00083-X

background of this work is the prediction of the deposition flux of droplets for horizontal annular dispersed gas/liquid flows. Fig. 1 shows the entrainment/deposition-mechanism in a horizontal annular dispersed gas/liquid flow.

Droplets can entrain from the liquid film, enter the turbulent gas core and after some time they can deposit on some place on the annular liquid film. This is one of the mechanisms that have been proposed to explain the annular character of the film (Fukano and Ousaka, 1989; Laurinat et al., 1985; Mols, 1999). In this paper we focus on the prediction of the deposition flux for droplets up to a diameter of 200 μm. The motion of larger droplets is almost totally determined by the influence of gravity and the initial velocity with which a droplet is entrained from the liquid film. Droplets between 120 and 200 μm are both influenced by turbulence and by gravity, and still form a significant part of the droplet size distribution in a horizontal annular dispersed gas/liquid flow (Mols, 1999).

Binder and Hanratty (1992) use a one-dimensional Turbulent Diffusion-model to calculate dispersion and deposition of particles in a channel flow. They solve a one-dimensional convection/diffusion-equation numerically, while simultaneously solving an equation for the time-evaluation of the particle deterministic gravitational settling velocity. The diffusion part of the convection/diffusion-equation represents the influence of the turbulent eddies, whereas the convective part represents the influence of gravity on the particles. Particles are emitted with a certain initial velocity from an instantaneous source at the bottom and can deposit at either of the perfectly absorbing walls. They use a time-dependent diffusivity and free fall velocity, and calculate instantaneous and fully developed concentration profiles, as well as deposition rates and deposition constants.

The method used by Mols and Oliemans (1998) differs from the approach of Binder and Hanratty (1992) in two aspects. First, the particle diffusion coefficient and the gravitational

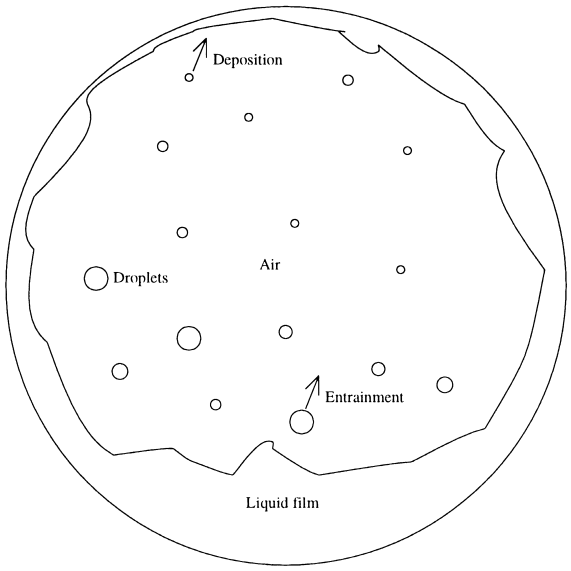

Fig. 1. The entrainment/deposition-mechanism in a horizontal tube.

settling velocity are assumed to be time-independent by Mols and Oliemans. This assumption has the advantage that the one-dimensional problem then can be solved analytically. It furthermore has the advantage that an analytical two-dimensional deposition flux in a tube can be calculated which contains the relevant physical parameters of the problem that are hidden in generally used empirical correlations: the Stokes-number and the Froude-number. The Stokes-number S is the ratio of the particle time scale τ_p and the fluid time scale T_L, characterising the response of particles on the fluid turbulence. The Froude-number Fr^* is defined as $(u^*)^2/gH$, where u^* is the friction velocity, g the acceleration of gravity and H the height of the channel. Second, Mols and Oliemans (1998) use a particle diffusion coefficient that is equal to the fluid diffusivity for Stokes numbers smaller than one, but that decreases relative to the fluid diffusivity with increasing Stokes number. This is contrary to previously used models for annular flows, where a particle diffusivity equal to the fluid diffusivity was used (Vames and Hanratty, 1988; Lee et al., 1989b; Paras and Karabelas, 1991; Binder and Hanratty, 1992; Hay et al., 1996).

Mols and Oliemans (1998) also extended the one-dimensional analytical result for the deposition flux of particles to two dimensions by assuming that the concentration on a horizontal line is constant. In the two-dimensional Turbulent Diffusion-model that is presented in this paper, a two-dimensional deposition flux can be explicitly calculated without any assumption on the particle concentration.

Lee et al. (1989a) have considered a two-dimensional Turbulent Diffusion-model for a vertical tube-flow. This case differs from the problem that we consider in this paper because there is no gravity present. The two-dimensional diffusion-equation in cylindrical coordinates can then be solved analytically, whereas for a horizontal tube flow gravity causes the problem to be asymmetric, so that no analytical solution can be found. Therefore a numerical method is used in this paper to solve the two-dimensional convection/diffusion-equation. The biggest advantage of the two-dimensional model that we present in this paper is that any arbitrary arrangement of droplet sources along the tube circumference can be considered, so that much more realistic concentration profiles and deposition fluxes can be calculated than in a one-dimensional model.

The rest of this paper is organised as follows. In section 2 we present the two-dimensional Turbulent Diffusion model. Section 3 contains the main results that we have got from the two-dimensional Turbulent Diffusion-model. Finally, the most important conclusions are drawn in section 4.

2. The two-dimensional Turbulent Diffusion-model

2.1. Convection/diffusion-equation in cylinder coordinates

The Turbulent Diffusion (TD)-model and its assumptions have been extensively defined in Mols and Oliemans (1998). For the two-dimensional model the definition of the model and its assumptions are still the same. The most important assumptions are that the turbulence is assumed to be homogeneous (up to a small near wall region where the fluid r.m.s. velocity rapidly goes to zero) and that particles move in the streamwise direction at the same velocity

as the fluid. The streamwise fluid velocity is assumed to be uniform and the tube wall is perfectly absorbing. The relevant length and time scales of the problem under consideration are given in Tables 1 and 2.

We consider the problem of dispersing and depositing particles in the two-dimensional cross-section of a tube. The general convection-diffusion-equation describing the particle dispersion in a turbulent flow in the presence of gravity is then given by:

$$\frac{\partial C}{\partial t} + (v_g \cdot \nabla)C = \nabla \cdot (D_\mathrm{p} \nabla C). \tag{1}$$

C is the particle concentration, t is the time, D_p the particle diffusion coefficient and v_g the convective particle velocity due to gravity, i.e. the particle free fall velocity. The stationary value of v_g equals $g\tau_\mathrm{p}$, where g is the acceleration of gravity and τ_p the particle relaxation time. D_p and v_g can be time-dependent. D_p can also be spatial-dependent or even anisotropic. Using cylinder-coordinates (r, ϕ) and making use of the approximation that the velocity field is divergence free ($\bigtriangledown \cdot v_g = 0$), Eq. (1) can be written in conservative form:

$$\frac{\partial C}{\partial t} + \frac{1}{r}\frac{\partial ruC}{\partial r} + \frac{1}{r}\frac{\partial vC}{\partial \phi} = \frac{1}{r}\frac{\partial}{\partial r}\left[rD_\mathrm{p}\frac{\partial C}{\partial r}\right] + \frac{1}{r}\frac{\partial}{\partial \phi}\left[\frac{D_\mathrm{p}}{r}\frac{\partial C}{\partial \phi}\right] \tag{2}$$

u is the convective velocity component in the r-direction and v the convective velocity component in the ϕ-direction. Eq. (2) is made dimensionless in the same way as in Binder and Hanratty (1992):

$$r^+ = \frac{r}{R};\ D_\mathrm{p}^+ = \frac{D}{u^* R};\ u^+ = \frac{u}{u^*};\ t^+ = \frac{tu^*}{R};\ C^+ = \frac{Cu^*}{R_\mathrm{E}};\ v^+ = \frac{v}{u^*}. \tag{3}$$

u^* is the friction velocity, R_E is the average rate of droplet entrainment in kg/(m^{2}s) and R is the radius of the tube. The form of the equation in dimensionless quantities is identical to Eq. (2).

The boundary condition that we apply is the so called diffusion-free flight-boundary condition: High-inertia particles are assumed to reach the boundary layer by turbulent diffusion and to pass through the boundary layer by a so called free flight process (Mols and Oliemans, 1998). The boundary condition in cylinder coordinates is formulated as

$$-D_\mathrm{p}\frac{\partial C}{\partial r}\bigg|_\mathrm{R} = \nu C_\mathrm{R}, \tag{4}$$

where C_R is the concentration at the wall and $\frac{\partial C}{\partial r}|_\mathrm{R}$ the gradient of the concentration at the

Table 1
Length scales

Tube diameter	5×10^{-2} m
Eulerian eddy length scale	5×10^{-3} m
Kolmogorov length scale	$\mathcal{O}$ (100) μm
Particle diameter	10 μm $< d_\mathrm{p} <$ 200 μm

wall. This is a phenomenological way of modelling the perfectly absorbing boundary condition in terms of the particle concentration. The free flight velocity ν is calculated by:

$$\nu = \frac{1}{2}\sqrt{\frac{2}{\pi}}\sqrt{\left\langle (v_p')^2 \right\rangle}, \tag{5}$$

where the mean square fluctuating particle velocity $\langle (v_p')^2 \rangle$ is calculated according to Hinze (1975)

$$\frac{\left\langle (v_p')^2 \right\rangle}{\left\langle (v_f')^2 \right\rangle} = \frac{1}{1+S}. \tag{6}$$

$\langle (v_f')^2 \rangle$ is the mean square fluctuating fluid velocity and S the particle Stokes-number.

2.2. Modelling the particle diffusion coefficient

Having introduced the mathematical model for the convection-diffusion problem, we now need a physical model for the particle diffusion coefficient. In previous models and measurements of particle dispersion in annular flows (Vames and Hanratty, 1988; Lee et al., 1989b; Paras and Karabelas, 1991; Binder and Hanratty, 1992; Hay et al., 1996) it was presupposed or concluded that the diffusivity of particles is roughly equal to or larger than the diffusivity of the fluid. Although Lee et al. (1989b) find for 150 μm particles a significantly reduced particle diffusivity with respect to the fluid, they contribute this either solely due to gravity or to the fact that particles have not been long enough in the flow, presupposing that they should find particle diffusivities equal to the ones for homogeneous isotropic stationary turbulence. Vames and Hanratty (1988) found for 90 μm particles also a reduced particle diffusivity, but contribute this to an experimental error as they did not find reduced particle diffusivities for lower inertia particles.

The presupposition that the particle diffusivity is roughly equal to the fluid diffusivity is based on experimental and theoretical results for homogenous isotropic turbulence (Reeks, 1977; Pismen and Nir, 1978). However, in Mols (1999) it was shown that there is an important difference between results in homogeneous isotropic stationary turbulence (without a mean flow) and the results in bounded flows where a mean flow is present. There it is shown that the wall normal particle diffusivity decreases with increasing particle inertia for wall bounded flows driven by a pressure gradient. This is a combination of three effects: (1) crossing trajectories effect plus the related continuity effect due to the velocity difference between particle and fluid in the streamwise direction; (2) bounded flows lead to limited length and time scales compared

Table 2
Time scales

Integral fluid time scale	$\mathcal{O}(10^{-3})$ s
Particle relaxation time ($d_p = 10$ μm)	$\mathcal{O}(10^{-4})$ s
Particle relaxation time ($d_p = 200$ μm)	$\mathcal{O}(10^{-1})$ s

with homogeneous isotropic flows; and (3) crossing trajectories effect due to gravity for a horizontal flow, and crossing trajectories plus continuity effect for a vertical flow.

Both the crossing trajectories effect and the continuity effect caused by gravity have been investigated by Csanady (1963). The crossing trajectories effect is related to the fact that in the presence of a large drift velocity the fluid time scale seen by the particle is reduced. The continuity-effect is the effect that a particle that is falling through an eddy, let us assume in the z-direction, and first experiences fluid velocities in, let us assume, the *plus*-x-direction, next experiences fluid velocities in the *minus*-x-direction: the particle falls into the backflow of the eddy. The dispersion in the x-direction is thus reduced. Whereas the crossing trajectories effect works equally in all directions, the continuity-effect only works in the direction *normal* to the drift velocity. Although the continuity effect is physically inseparable from the crossing trajectories effect, it is for conceptual purposes illustrative to separate them. More details of these effects can be found in Mols (1999). As the streamwise particle velocity in annular flows is about 20% smaller than the streamwise fluid velocity (Azzopardi, 1997), effect (1) can reduce particle diffusivity up to 60% (for $S = 80$), even without a crossing trajectories effect caused by gravity (Mols, 1999).

The model for the particle diffusivity that we use in this paper is the same as the one used in Mols and Oliemans (1998). It is partly based on LES-data for particle diffusivity in a tube flow (Uijttewaal and Oliemans 1996), implicitly taking into account the first two of the three before mentioned effects, and partly on a theoretical analysis by Csanady (1963), taking into account the third effect. As in Mols and Oliemans (1998) the particle diffusivity D_p is related to the fluid diffusivity D_f according to:

$$D_\mathrm{p} = \gamma_v \gamma_g D_\mathrm{f}. \tag{7}$$

The fluid diffusivity is given by (Taylor, 1921):

$$D_\mathrm{f} = \int_0^\infty \left\langle v_\mathrm{f}'(0) v_\mathrm{f}'(t) \right\rangle \mathrm{d}t = \left\langle (v_\mathrm{f}')^2 \right\rangle T_\mathrm{L}, \tag{8}$$

where v_f' is the fluctuating velocity of the fluid. The fluid mean square velocity is approximated by

$$\left\langle (v_\mathrm{f}')^2 \right\rangle = (0.7u^*)^2. \tag{9}$$

For the term γ_v we write again:

$$\gamma_v = \frac{1}{\sqrt{1 + (\tau_\mathrm{p}/T_\mathrm{L})}}. \tag{10}$$

The factor γ_v is the results of the before mentioned effects (1) and (2). It should be noted that Eq. (10) is the result of a rough fit to LES-data for a tube flow (Uijttewaal and Oliemans, 1996) and that it is not a result of some theoretical analysis of the effects (1) and (2) on the particle diffusivity. We have now used the notation γ_v instead of γ_inert (Mols and Oliemans, 1998) because, although the term depends on the particle inertia, the physical cause for the reduction of the particle diffusivity is mainly the crossing trajectories effect plus the related

continuity effect induced by the velocity difference in streamwise direction between particle and fluid (Mols, 1999).

The presence of a gravity causes another crossing trajectories effect that has already been recognised by Csanady (1963). γ_g is the result of this third effect, where the subscript g now denotes that this crossing trajectories term is caused by gravity. The crossing trajectories coefficient γ_g is then given by (Mols and Oliemans, 1998):

$$\gamma_g = \frac{1}{\sqrt{1 + \left(\frac{g\tau_p T_L}{\mathscr{L}}\right)^2}}. \tag{11}$$

The crossing trajectories effect due to gravity starts to reduce the particle diffusivity when the free fall velocity is of the order of, or larger than, the magnitude of the fluid r.m.s. velocity. This is for particles approximately larger than 140 μm (Mols and Oliemans, 1998). For situations where the free fall velocity is significantly smaller than the fluid r.m.s. velocity, the effect is negligible. In the simulations that we have performed, the particles are smaller than 140 μm and v_g is smaller than the fluid r.m.s. value except for the case $S = 100$, $Fr^* = 10$. Therefore the crossing trajectories factor due to gravity is not taken into account in the present calculations.

Whereas Binder and Hanratty (1992) use a time-dependent particle diffusivity, we use a time-independent one, only for reasons of simplicity. The numerical method of solution (Finite Volume Method) that we use to solve the two-dimensional convection/diffusion-problem (2) with the boundary condition (4) and some chosen initial condition is explained in Mols (1999). This method can still be used if the particle diffusivity and the particle deterministic fall velocity are time-dependent.

3. Results

This section presents the results of the two-dimensional TD-model. First a comparison is made between results from our two-dimensional model and results from the one-dimensional TD-model of Binder and Hanratty (1992) with a single source of droplets at the bottom as initial condition. Second, contour plots for the concentration in the tube-cross section resulting from multiple initial sources of droplets are compared with experimental results for droplet fluxes in horizontal annular dispersed gas/liquid flow. Finally, a fully developed quasi-stationary flow is simulated and a two-dimensional deposition flux is calculated for different values of S and Fr^*.

3.1. Comparison between one- and two-dimensional TD-results

Binder and Hanratty (1992) have calculated concentration profiles for different combinations of S and Fr^* in a one-dimensional model with an instantaneous source of droplets at the bottom wall as initial condition. For the same combinations of S and Fr^*, and for the same

initial concentration (an instantaneous source of droplets at the bottom of the tube), we have calculated concentration profiles along the vertical diameter of the tube cross-section.

Before comparing the results from the two-dimensional TD-model with results from the one-dimensional TD-model of Binder and Hanratty, we first summarise the differences between these two models. Apart form the difference in the geometry, we use (1) a different model for the particle diffusion coefficient (see Section 2.2), (2) we do not use an initial entrainment velocity, (3) we use a stationary fall velocity instead of a time-dependent one and (4) we use a stationary particle diffusivity instead of a time-dependent one.

The differences (1), (2) and (3) are expected to lead to particles reaching lower positions in our two-dimensional model as compared to the model of Binder and Hanratty. Difference (4) leads to particles reaching higher positions in the tube flow. These two effects are competing. In Table 3 it is seen that for all the times the particle diffusivity used in the two-dimensional model is smaller than the corresponding one in the one-dimensional model. D_{pBH} is the particle diffusivity used by Binder and Hanratty and $D^{\infty}_{\mathrm{pBH}}$ is the stationary value of this particle diffusivity. In this table we have calculated the value of $D_{\mathrm{pBH}}/D_{\mathrm{f}}$ for all the three moments in time: $x/H = 10$, 20, 30, according to:

$$D_{\mathrm{pBH}}(t) = D_{\mathrm{f}}\left[1 - \exp\left(-\frac{t}{\tau_{\mathrm{p}}}\right)\right]. \tag{12}$$

x/H is the ratio between the distance travelled downstream by the particles and the channel height. The distance travelled downstream in the channel is equal to the time multiplied by the average gas velocity. For $S = 1$, the stationary particle diffusivity is reached very rapidly. Only for $S = 100$, $Fr^* = 10$ it is very important to take the time-dependency of the particle diffusivity into account.

In Figs. 2, 4, 6 and 8 results of the two-dimensional TD-model are given for the same Stokes and Froude-numbers as Binder and Hanratty used in their one-dimensional TD-model: $S = 1$, $S = 100$ and $Fr^* = 10$, $Fr^* = 100$. The particle and fluid characteristics that we use are listed in Table 4. The results of Binder and Hanratty are given in Figs. 3, 5, 7 and 9. The concentration profiles for the two-dimensional model are shown for three different distances travelled downstream in the tube: $x/R = 10$, 20, 30, where R is the tube diameter. They are compared with the corresponding concentration profiles in the channel flow for $x/H = 10$, 20, 30, where H is the channel height. We will compare the results of the two models qualitatively.

Three conclusions can be drawn from all the results. First there is a striking difference

Table 3
Particle Stokes number (S), particle relaxation time (τ_{p}), fluid Froude-number (Fr^*). The last three columns give $D_{\mathrm{pBH}}/D^{\infty}_{\mathrm{pBH}}$ at three moments in time

S	τ_{p}(s)	Fr^*	$x/H = 10$	$x/H = 20$	$x/H = 30$
1	7.0×10^{-4}	10	1	1	1
1	5.1×10^{-5}	100	1	1	1
100	7.0×10^{-2}	10	0.2	0.3	0.4
100	5.1×10^{-3}	100	0.91	0.99	1

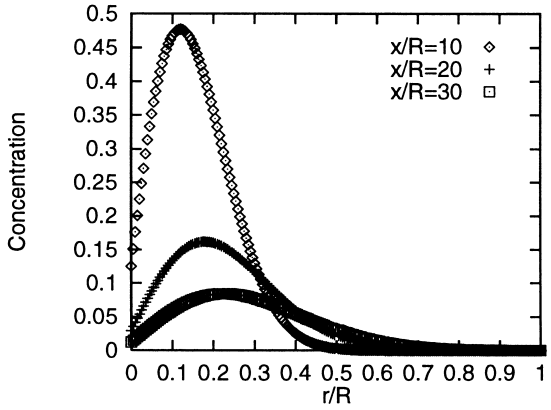

Fig. 2. Concentration profiles (scaled with the initial concentration) on the vertical centre-line, calculated in the two-dimensional TD-model; $S = 1$ and $Fr^* = 10$; R is the tube diameter.

in the behaviour of the concentration profile at the bottom wall. From Eq. (4) it follows that the gradient of the concentration at the wall is determined by the ratio v/D_p. The free flight velocity v that we use is the same as the one used by Binder and Hanratty, but the particle diffusivity that we use is smaller than the stationary ones used by Binder and Hanratty as can be seen in Table 4. Even if we take into account that the particles in the channel flow have a time-dependent diffusivity, the diffusivities used in the two-dimensional TD-model are smaller than the corresponding ones for the channel flow, as was seen in Table 3. This leads to a larger ratio v/D_p, and thus to a larger gradient in the concentration at the wall. Second, despite the a priori expectation that in our two-dimensional model particles are expected to come not as high as in the one-dimensional model, the opposite is found for the cases $S = 1$ & $Fr^* = 10$, $S = 1$ & $Fr^* = 100$ and $S = 100$ & $Fr^* = 100$. The only cause that is left to explain this result, is the fact that we consider diffusion of particles in two dimensions instead of in one

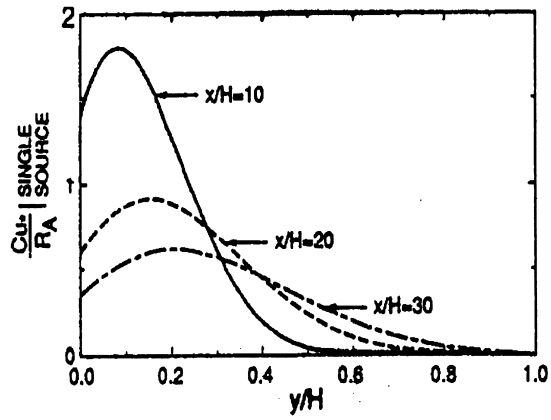

Fig. 3. Concentration profiles calculated by Binder and Hanratty for $Fr^* = 10$ and $S = 1$; with initial velocity; R_A is a constant value equal to the entrainment rate.

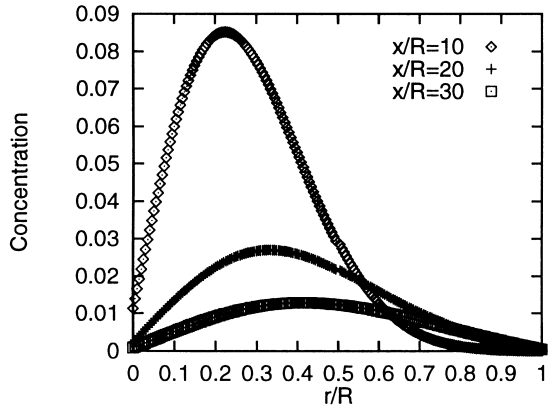

Fig. 4. Concentration profiles (scaled with the initial concentration) on the vertical centre-line, calculated in the two-dimensional TD-model on the vertical centre-line; $S = 1$ and $Fr^* = 100$; R is the tube diameter.

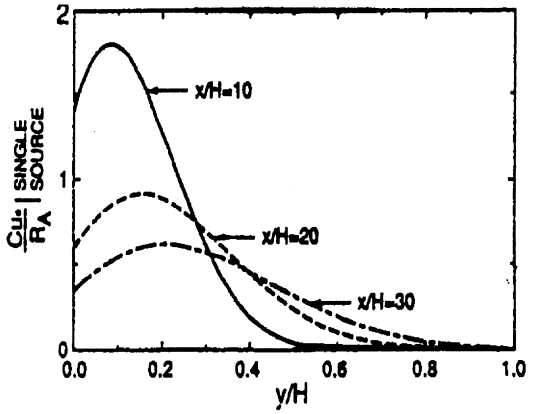

Fig. 5. Concentration profiles calculated by Binder and Hanratty for $Fr^* = 100$ and $S = 1$; with initial velocity; R_A is a constant value equal to the entrainment rate.

Table 4
Particle Stokes number (S), particle relaxation time, fluid Froude-number (Fr^*), particle diffusion coefficient (D_p) used in two-dimensional TD-model, and particle diffusion coefficient (D_{pBH}) used by Binder and Hanratty

S	τ_p	Fr^*	D_p (m^2/s)	$D_{pBH} = D_f$ (m^2/s)	$D_p D_{pBH}$
1	7.0×10^{-4}	10	1.18×10^{-3}	1.68×10^{-3}	0.70
1	5.1×10^{-5}	100	8.60×10^{-4}	1.22×10^{-3}	0.70
100	7.0×10^{-2}	10	1.67×10^{-4}	1.68×10^{-3}	0.10
100	5.1×10^{-3}	100	1.21×10^{-4}	1.22×10^{-3}	0.10

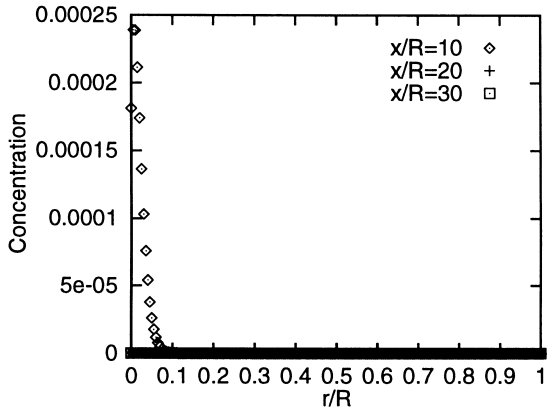

Fig. 6. Concentration profiles (scaled with the initial concentration) on the vertical centre-line, calculated in the two-dimensional TD-model; $S = 100$ and $Fr^* = 10$; R is the tube diameter.

dimension. Only for $S = 100$ & $Fr^* = 10$ particles reach higher positions in the channel. Third, the total particle concentration decreases slightly more rapid then in the one-dimensional model. This leads to a larger deposition coefficient in the two-dimensional model, because particles are more influenced by the presence of the wall in a tube than in a channel.

The two-dimensional TD-results show that the concentration profiles for increasing Froude-numbers, i.e. a larger influence of turbulent diffusion, differ from each other as is expected. Binder and Hanratty, however, found in their one-dimensional TD-model the same concentration profiles for the combination $S = 1$, $Fr^* = 10$ as for the combination $S = 1$, $Fr^* = 100$: Figs. 3 and 5 are exactly equal. This cannot be due to the different model for the particle diffusivity, since the particle diffusivity used in the two-dimensional model is smaller than the one used by Binder and Hanratty. The determination of the free flight velocity is the

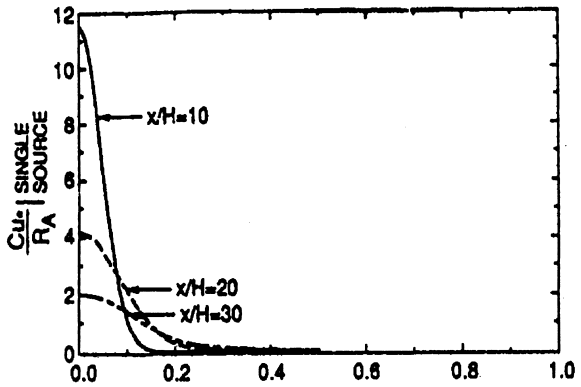

Fig. 7. Concentration profiles calculated by Binder and Hanratty; $Fr^* = 10$ and $S = 100$; with initial velocity; R_A is a constant value equal to the entrainment rate.

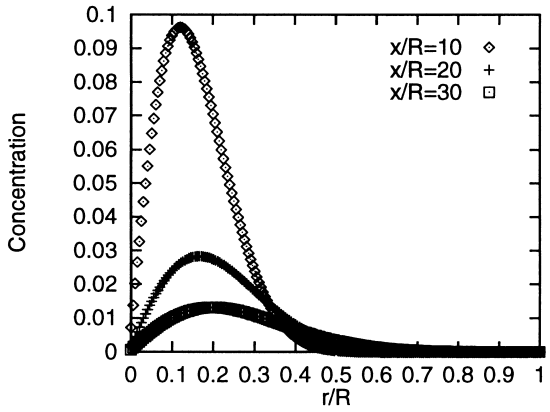

Fig. 8. Concentration profiles (scaled with the initial concentration) on the vertical centre-line, calculated in the two-dimensional TD-model; $S = 100$ and $Fr^* = 100$; R is the tube diameter.

same for both the one-dimensional and the two-dimensional TD-model. It is not understood why the one-dimensional TD-model of Binder and Hanratty gives the same concentration profiles for $S = 1$, $Fr^* = 10$ and for $S = 1$, $Fr^* = 100$.

To finish this section we now consider the particle concentration in the whole cross-section of the tube for the case $S = 30$, $Fr^* = 50$. As initial condition we have again used a single source at the bottom of the tube.

Figure 10 shows the contour plot of the concentration of particles along the vertical diameter. The lines shown are the iso-concentration lines, connecting points with an equal particle concentration. In the middle of the inner circle the concentration is the highest and at the walls the concentration is almost zero. Fig. 11 shows the concentration on a vertical line through the centre. The global maximum in the concentration profile corresponds to the

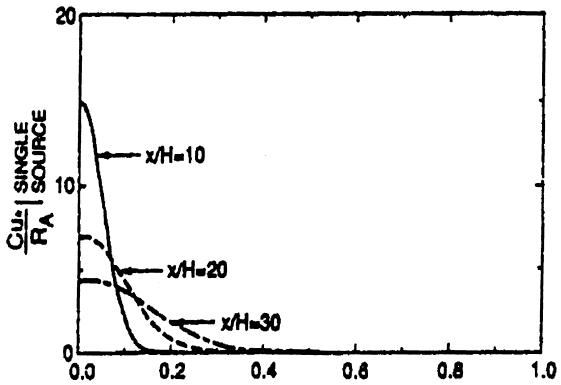

Fig. 9. Concentration profiles calculated by Binder and Hanratty; $S = 100$ and $Fr^* = 100$; with initial velocity; R_A is a constant value equal to the entrainment rate.

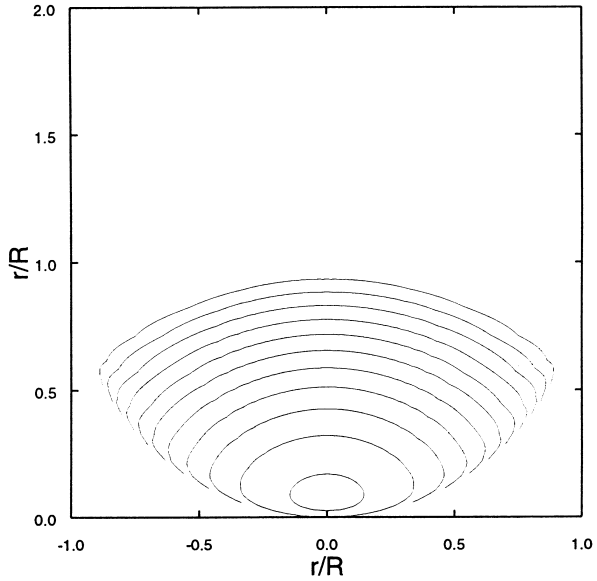

Fig. 10. Contour plot for $S = 30$, $Fr^* = 50$. Iso-concentration lines from top to bottom: 1×10^{-11}, 1×10^{-10}, etc. till 0.1.

midpoint of the small circles in the contour plots. It is seen that no particles are present in the upper half of the tube.

3.2. Multiple annular particle sources

In the previous section the time-dependency of the particle concentration resulting from a single source of particles at the bottom was studied. Annular flow, however, can be considered as the sum of a lot of these sources both distributed along the tube wall, and in the streamwise direction. The advantage of the two-dimensional TD-model that we have introduced is that we

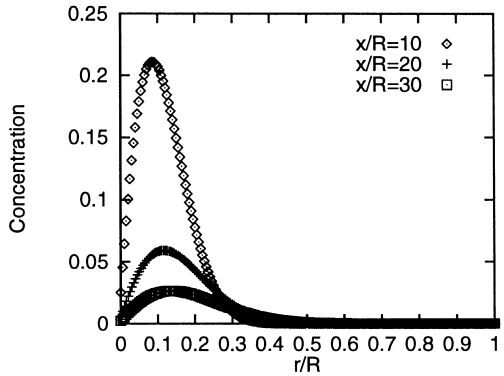

Fig. 11. Concentration profiles (scaled with the concentration) on the vertical centre-line for $S = 30$ and $Fr^* = 50$.

can put sources on arbitrary places along the tube wall. As the effect of sources placed along a tube wall has not been investigated before, this is the subject of the present section.

To mimic droplet entrainment from a liquid film with varying thickness, we now consider in our two-dimensional model initial sources that are distributed all around the tube wall in each grid cell located at the wall. The intensity of these sources decreases towards the top in two steps: For $0 < \phi < \frac{5}{12}\pi$ the initial concentration is arbitrarily chosen as $C^+_{\text{init}} = 20$ in each grid cell. For al the gridpoints within $\frac{5}{12}\pi < \phi < \frac{5}{6}\pi$, $C^+_{\text{init}} = 10$, and for all the gridpoints within $\pi < \phi < \frac{5}{6}\pi$, $C^+_{\text{init}} = 5$. As there is little experimental information available on the strength of the droplet sources, we want to investigate in the first place the qualitative effect of an annular distribution of sources with decreasing strength towards the top. If u^* is of the order of 1 m/s, and a typical entrainment rate R_E in annular flow is of the order of 0.1 kg/(m^2 s) (Azzopardi, 1997), then it follows form Eq. (3) that a dimensionless concentration of 20 corresponds to a physical concentration of 2 kg/m^3. Concentrations measured by Paras and Karabelas (1991) at the bottom wall vary between 0.4 and 2.6 kg/m^3 depending on the liquid and gas velocity that are used.

Besides an annular distribution of droplet sources, we also add the contribution of three annular line sources placed upstream. For the moment we consider the concentration distributions resulting from annular line sources placed at three different positions upstream: x/R = 10, 30 and 90. The total concentration profile that we calculate is the result of three annular line sources placed at different positions upstream for two particle types, S = 1 and S = 21, corresponding to 20 and 100 μm particles. In Fig. 12 the result from this first approximation of quasi-stationary annular flow is shown.

In Fig. 13 a three-dimensional plot of the concentration in the tube is shown for 20 and 100 μm particles with initial sources all around the tube wall and at three positions the upstream direction. The global maximum and the local minimum can be clearly seen. The increase of droplet concentration towards the wall is due to the annular initial source distribution.

We now want to make a qualitative comparison between these two-dimensional results for the particle concentration and experimental results from Williams et al. (1996) for a horizontal annular dispersed gas/liquid flow in a tube with a diameter of 9.53 cm. Fig. 14 shows a result of experiments by Williams et al. (1996) for the particle flux in a horizontal annular dispersed gas/liquid flow. It should be noted that in these experiments not only the deposition-mechanism is present but that the particle flux that is shown can also be influenced by the entrainment along the wall and by the secondary gas flow. In these experiments an axial flux of droplets was measured. This flux is equal to the concentration multiplied by the velocity of the droplets in the streamwise direction. In the TD-model it is assumed that the average fluid velocity (as well as the average particle axial velocity) is constant over the whole cross-section of the tube, which means that the concentration should be multiplied with the uniform gas velocity in order to get the particle flux. However, measurements of Dykhno et al. (1994) in a horizontal 9.53 cm tube indicate a more or less parabolic axial average fluid velocity profile, with a lower average velocity in the lower half (due to the larger shear at the more wavy bottom interface) and a higher average velocity in the upper half (due to the less wavy top interface). For a small amount of atomisation the top of the parabola lies in the bottom part of the tube, whereas for a large amount of atomisation the top shifts to the upper part of the

tube. This velocity profile should be taken into account when interpreting the measured values for the droplet flux in terms of droplet concentration.

As the value of the concentration also depends on the unknown initial source strengths, the results for the measured particle fluxes can not be compared quantitatively with the particle concentrations for the two-dimensional model. Qualitatively, however, a comparison can be made between the two-dimensional concentration profiles and the fluxes measured by Williams et al. (Fig. 14).

Comparing the results shown in the Figs. 12 and 13 with the experimental result shown in Fig. 14 we notice that in both cases the droplet concentration increases when going to the walls. For the experimental results this might partly be due to the presence of droplets sources at the wall, and partly due to a secondary gas flow in the upward circumferential direction at the wall. For the two-dimensional result this can only be due to the annular source distribution that was assumed. Looking at the central part of the flow, we see that in both cases a local maximum is found. In both the experimental results and in the TD-results there is a circle in the central part with a lower concentration than the surrounding flow. Above this local minimum, there is a local maximum. There is also an important difference. In the result of Williams et al. the local maximum lies at two sides of the vertical centre line. Probably, a secondary gas flow, with two cells in the plane of a tube cross-section, is responsible for splitting a single local maximum into two. But the local maximum that occurs at $y/R = 0.6$ in Fig. 14 can also be explained by the fact that the distribution of droplet sources has got more

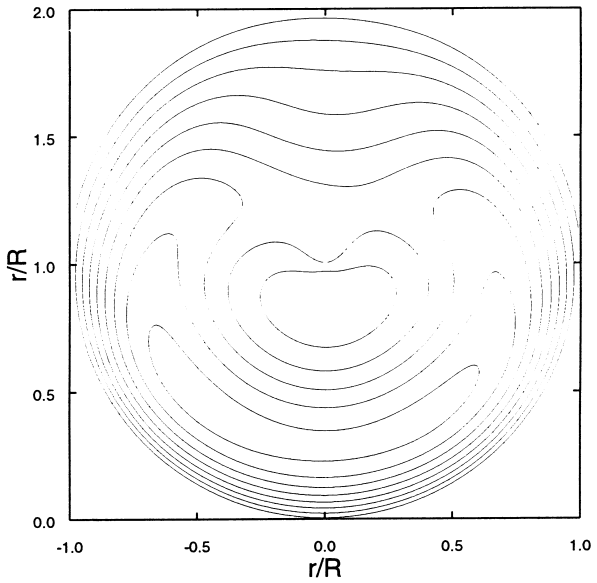

Fig. 12. Contour plots for the summed contribution of $S = 1$ and $S = 21$, $Fr^* = 5$ (20 and 100 μm particles) with several sources all around the tube wall and in the flow direction. The circle above the centre point is a local minimum (0.12), the inner circle at the bottom half is the maximum (0.2). Concentration levels from 0.04–0.2 in steps of 0.02. The circle in the centre has the same value as the fifth line counted from the top of the tube.

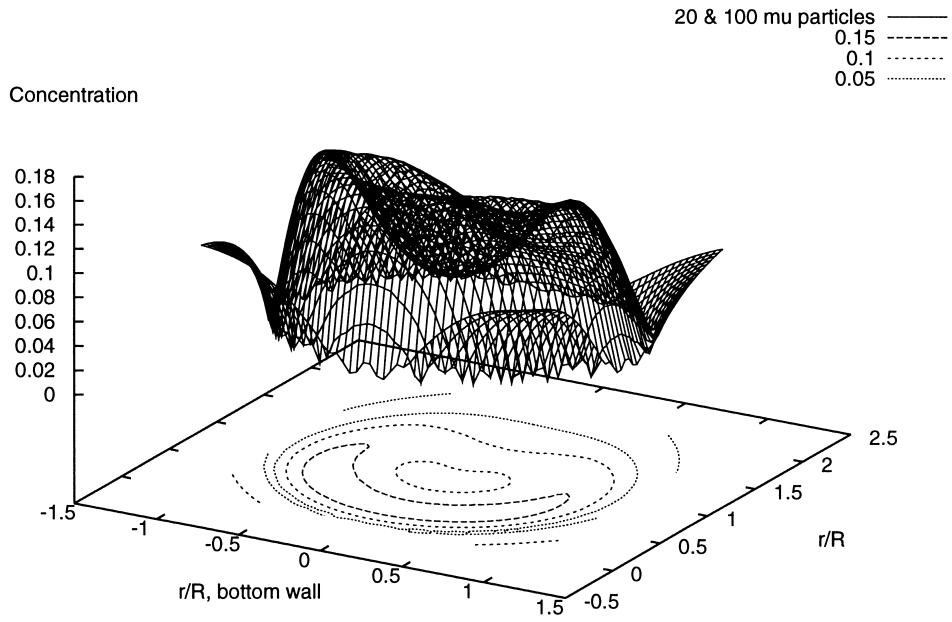

Fig. 13. Three-dimensional concentration profile for the combination of 20 and 100 μm particles. Three initial annular sources in the stream wise direction. R is the tube radius. The global maximum and the local minimum are visible as well as the particle increase towards the walls.

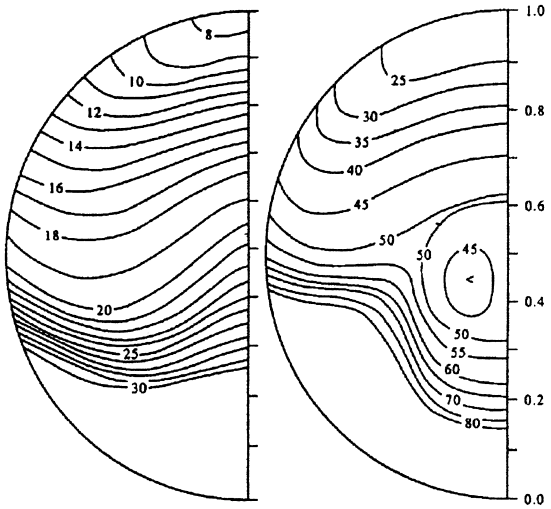

Fig. 14. Experimental results of Williams et al. (1996) for the particle flux (kg/m^2 s). In the left part of the figure the gas velocity is 33 m/s and in the right part of the figure the gas velocity is 45 m/s.

annular for 45 m/s gas velocity than for 33 m/s gas velocity and is not necessarily due to the presence of a secondary gas flow as Williams et al. stated.

Fig. 15 shows two concentration profiles for two different gas velocities as measured by Paras and Karabelas (1991). Whereas there is no local maximum for a gas velocity of 30 m/s, a clear local maximum is found for 45 m/s gas velocity. The drawn lines are the result of a one-dimensional model. It is seen that a one-dimensional model is not able to predict the local maximum in the concentration. This is in accordance with our hypothesis that the local maximum is the result of the fact that the liquid film is more annular at 45 m/s than at 30 m/s, so that droplets start to entrain along a large part of the tube circumference. For 30 m/s the entrainment of droplets is only at the bottom of the tube and no local maximum is found, as there were no local maxima in the concentration profiles of Section 3.1.

It is not expected that the local maximum for 45 m/s gas velocity is due to secondary gas flow, as the influence of the secondary gas flow decreases with increasing gas velocity. However, the local maximum might partly be caused by the average axial gas velocity profile that shows a maximum in the upper part of the tube at high gas velocities (Dykhno et al., 1994). The concentration shown in Fig. 15 is calculated from the measured particle flux divided by a uniform gas velocity. The assumption of a uniform gas velocity leads to an overprediction of the concentration in the top part if the real gas velocity profile shows a maximum in the top part.

3.3. Simulation of a fully developed horizontal annular dispersed gas/liquid flow

In the previous section the total concentration was calculated as the sum of the contributions of two particle sizes placed at three positions downstream of the tube (with some source distribution along the tube wall). Although this gave a first indication of the concentration profiles for a quasi-stationary two-dimensional annular flow, it is possible to simulate a fully developed horizontal annular dispersed gas/liquid flow. This is the subject of the present section. The method of adding the contributions of multiple initial sources placed at different

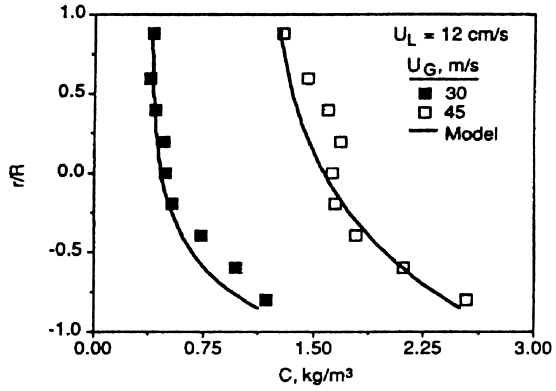

Fig. 15. Concentration profiles along the vertical diameter showing the local maximum in the concentration for $U_G = 45$ m/s and $r/R \approx 0.25$; R is the tube radius. Results obtained by Paras and Karabelas (1991).

positions upstream, has already been used by Binder and Hanratty (1992). Our two-dimensional model, however, has the advantage that at each upstream position an *annular line source* with an arbitrary arrangement of source strengths can be assumed, thus simulating the presence of an annular liquid film.

We now assume that droplets are mainly entrained from the tops of the roll waves that are present on the liquid film. The wavelength of these roll waves is approximately 100 times the height of the liquid film. Assuming a typical height of the liquid film at the bottom of 3 mm, roll waves will typically have a wavelength of 30 cm. Depending on whether or not the liquid film is fully annular (i.e. depending on the average gas velocity), sources should be distributed all along the tube wall (in the case of an annular liquid film) or up to a certain height (in the case of a partly annular liquid film). The total concentration $C(\mathbf{x}, t)$ at a position $\mathbf{x}$ at a time t is now given by

$$C(\mathbf{x}, t) = \sum_i \sum_\phi C_{i,\phi}\left(t' = \frac{x_j}{H}\right), \tag{13}$$

where $C_{i,\phi}$ $(t' = x_j/H)$ is the concentration of particles with a size i (starting at a circumferential angle ϕ) at a position $\mathbf{x}$ after a time (t') corresponding to x_j/H tube diameters travelled downstream. If we assume that the axial position $\mathbf{x}$ at which we want to calculate the concentration lies in the middle of two roll wave-tops, then:

$$x_j = \left(j - \frac{1}{2}\right)\lambda, \tag{14}$$

with λ the wavelength of a roll wave, and $j = 1, 2, 3\ldots$, denoting the jth roll wave-top counted in the upstream direction.

For our simulation of a fully developed annular dispersed gas/liquid flow we assume a particle size distribution as sketched in Fig. 4.1 in Mols (1999). We consider particles up to a diameter of 150 μm. For these particles the size distribution is approximately linear. We now cut the distribution in eight parts, each part corresponding with a certain particle diameter: 10, 30, 50, 70, 90, 110, 130 and 150 μm. In the upstream direction the annular line sources are distributed at 15 positions: $x/H = 3\ldots88$ in steps of $x/H = 6$, corresponding to the roll wave length of 30 cm. So, the first roll wave top occurs at $x/H = 3$, the second at $x/H = 9$, the third at $x/H = 15$, etc. The position $\mathbf{x}$ at which the concentration is determined, corresponds to the middle of two roll wave tops. The intensity of the sources on every annular line source decreases from bottom to top in the same way as described in Section 4.2.

Figs. 16–19 show the results for the 10, 50, 90 and 110 μm particles. We see that for the 10 μm particles the contour plots for the concentration show a single (global) maximum close to a part of the bottom wall. For the 50 μm particles there is a local maximum in the centre of the tube and the global maximum at the bottom has split into two parts. For the 90 μm particles there are two local maxima and for the 110 μm particles even three.

Fig. 20 shows the result for the approximated fully developed horizontal annular dispersed gas/liquid flow. Due to the distribution of sources all around the tube wall, the concentration at the wall is relatively high. There is a local maximum in the centre of the tube, and there are local maxima at the sides.

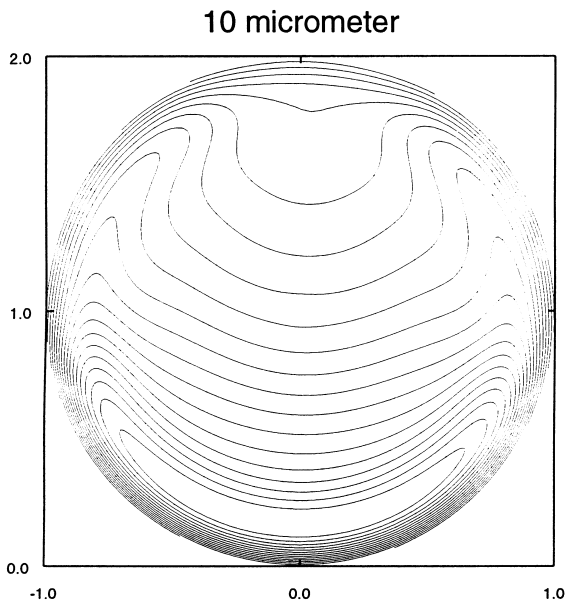

Fig. 16. Contour plot for the 10 μm particles showing only one (global) maximum.

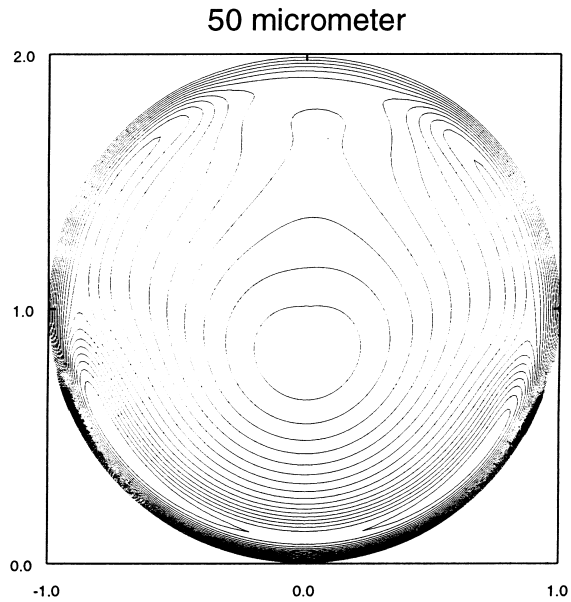

Fig. 17. Contour plot for the 50 μm particles with a global maximum almost on the bottom and a local maximum just below the tube centre.

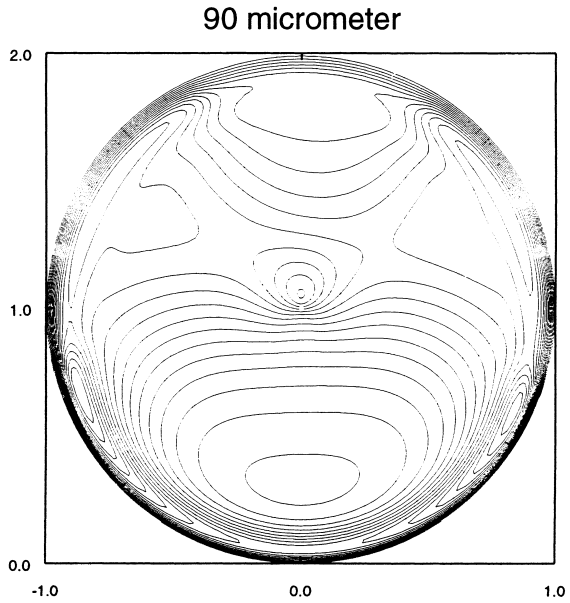

Fig. 18. Contour plot for the 90 μm particles with a global maximum at the bottom and two local maxima.

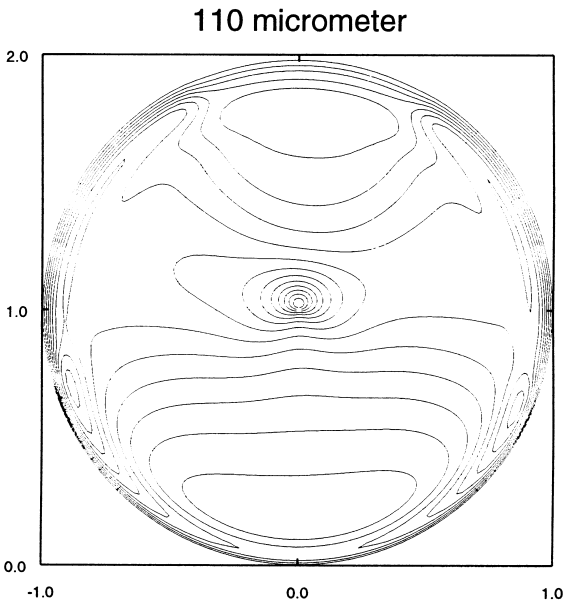

Fig. 19. Contour plot for the 110 μm particles with a global maximum at the bottom and two local maxima.

3.4. The two-dimensional deposition flux

In modelling a horizontal annular dispersed gas/liquid flow it is important to have an accurate expression for the particle deposition flux describing the amount of deposited material at a certain circumferential position (Mols, 1999). In our two-dimensional TD-model this deposition flux can be calculated explicitly.

Mols and Oliemans (1998) have derived a general form for the deposition flux by extending the analytical one-dimensional solution to a two-dimensional result, assuming that the concentration on a horizontal line is more or less constant. This assumption is based on experimental results of Paras and Karabelas (1991). The analytically derived deposition flux is given by:

$$R_{\mathrm{D}}(\phi,\ \tau_{\mathrm{p}}) = k_{\mathrm{D}}(\phi,\ \tau_{\mathrm{p}}) \cdot \ \exp\left(\frac{1}{4}P(\cos\phi - 1)\right). \tag{15}$$

P is the Peclet-number for the convection-diffusion problem (Mols and Oliemans, 1998) given by

$$P = \frac{g\tau_{\mathrm{p}}}{D_{\mathrm{p}}} \cdot 2R. \tag{16}$$

ϕ is the circumferential tube angle, defined to be 0 at the bottom. R is the radius of the tube. The Peclet-number characterises the ratio between the convective term due to gravity and the diffusive term due to turbulence. For $P \gg 1$ gravity is dominant and for $P \ll 1$ turbulent diffusion is dominant. $k_{\mathrm{D}}(\phi,\ \tau_{\mathrm{p}})$ is the local deposition constant and is defined as:

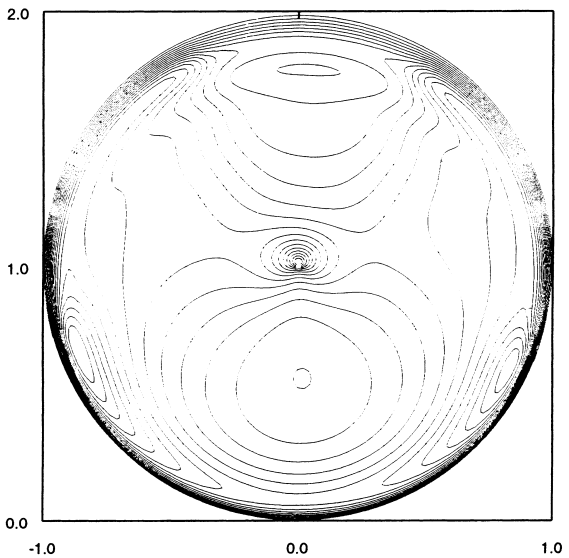

Fig. 20. Contour plot for the fully developed horizontal annular dispersed gas/liquid flow; addition of 8 different particle sizes and 15 upstream positions.

$$k_D(\phi, \tau_p) = c_E(\tau_p) \cdot (v + v_g \cos\phi). \tag{17}$$

The constant c_E can be determined from the fact that in a fully developed annular gas/liquid flow the total entrainment flux must equal the total deposition flux. This results in an expression for c_E:

$$c_E(\tau_p) = \frac{\int_0^\pi R_E(\phi, \tau_p)\, d\phi}{\int_0^\pi (v + v_g \cos\phi) \exp\left(\frac{1}{4}P(\cos\phi - 1)\right) d\phi} \tag{18}$$

c_E is used to normalise the deposition flux, and R_E is the rate of entrainment.

From the two-dimensional TD-results a deposition flux $R_D(\phi)$ can be calculated according to

$$R_D(\phi) = (v + v_g \cos\phi) \cdot C_{wall}(\phi), \tag{19}$$

$C_{wall}(\phi)$ is the concentration at a position (R, ϕ) at the wall.

How does the analytical expression (15) for the deposition flux compare with results of the two-dimensional model, where $R_D(\phi)$ can be explicitly calculated without the assumption that the concentration on a horizontal line is constant? We note that we can only make a qualitative comparison between the result of the two-dimensional model and the two-dimensional extension of the one-dimensional TD-model because the entrainment flux R_E is unknown. We make a comparison for the same S- and Fr^*-numbers as used by Mols and Oliemans (1998) in the one-dimensional model. Tables 5 and 6 give the various particle and fluid characteristics that are used in both models. As in the one-dimensional model, only a single initial source at the bottom wall is assumed.

In accordance with the numerical procedure that we have described, the deposition flux R_D can then be derived from the two-dimensional results as follows:

$$R_D(j, i) = \frac{(v^+ + u^+(j))C^+(j, i)}{C^+_{total}}, \tag{20}$$

C^+_{total} is the total concentration that is present in the tube. The calculation of the deposition flux is done for times when the profile has become quasi-stationary. Fig. 21 gives the result of the two-dimensional model. Fig. 22 gives the result of the model of Mols and Oliemans (1998). Comparing these two figures, we see that for $S = 0.2$ and $Fr^* = 4.6$ the ratio between the

Table 5
Properties of the fluid used for the calculation of the deposition flux: Froude-number; friction velocity; gas velocity; Lagrangian integral time scale; fluid mean square velocity

Fr^*	u^* (m/s)	V_G (m/s)	T_L (s)	$\langle(v'_f)^2\rangle$ (m^2/s^2)
4.6	1.5	32	1.6×10^{-3}	1.1
14.9	2.7	62	8.1×10^{-4}	3.57

Table 6
Properties of particles used for the calculation of the deposition flux: Stokes-number; Froude-number; particle mean square velocity; gravitational settling velocity; particle diameter; particle relaxation time

S	Fr^*	$\langle(v_p')^2\rangle$ (m^2/s^2)	v_g (m/s)	d_p (μm)	τ_p (s)
0.2	4.6	0.92	3.2×10^{-3}	10	3.2×10^{-4}
0.4	14.9	2.55	3.2×10^{-3}	10	3.2×10^{-4}
5.2	4.6	0.18	8.1×10^{-2}	50	8.25×10^{-3}
10.2	14.9	0.32	8.1×10^{-2}	50	8.25×10^{-3}
21	4.6	0.05	0.32	100	3.33×10^{-2}
41	14.9	0.085	0.32	100	3.33×10^{-2}

deposition flux at the top wall and the one at the bottom wall, is smaller for the two-dimensional TD-model than for the model derived by Mols and Oliemans. This might be a result of the assumption made in Mols and Oliemans (1998) that the concentration on a horizontal line is constant. It is expected that this slightly over estimates the concentration at the wall for these relatively small particles. If we look at Fig. 20 for the fully developed annular flow, we see that the latter result does not show horizontal iso-concentration lines. This is probably due to the absence of particles larger than 150 μm. These particles were not included in our calculations, whereas they do form a significant part of the particle size distribution. Furthermore, these 'heavy' particles are expected to be almost only influenced by gravity, so that they are expected to lead to horizontal iso-concentration lines.

The results of 50 μm particles are qualitatively the same for both models. 100 μm particles deposit up to one-half of the top in the two-dimensional model and only up to one-third in the one-dimensional model. For the 100 μm particles it is seen that the difference in the deposition flux for $Fr^* = 4.6$ and $Fr^* = 14.9$ is larger in the two-dimensional model than in the one-dimensional model.

In general it can be concluded that the deposition in flux in the semi-theoretical model shows

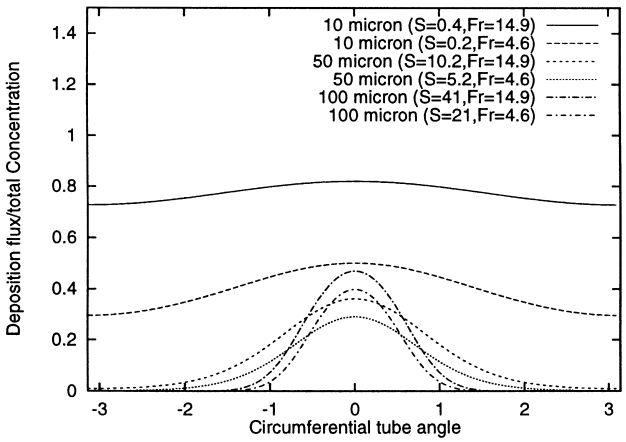

Fig. 21. Deposition flux for different S- and Fr^*-numbers calculated from the two-dimensional TD-results.

a good similarity with the calculated results of the two-dimensional TD-model. The two-dimensional TD-model, however, has given us for the first time the possibility to calculate two-dimensional concentration profiles and deposition fluxes without an additional assumption to extrapolate a one-dimensional result to a two-dimensional result.

For modelling horizontal annular dispersed gas/liquid flow it would be very useful to have an expression for the particle deposition flux expressed in the important dimensionless numbers, the Stokes-number and the Froude-number. To finish the present analysis of the particle deposition flux, we derive an expression for $R_D(\phi, S, Fr^*)$ and we analyse for which combination of S and Fr^* particles can deposit at the top of the tube. Annular flow model as presented in Fukano and Ousaka (1989) or Laurinat et al. (1985) use the dimensionless deposition flux R_D^+:

$$R_D^+ = \frac{R_D}{\rho_l u^*}. \tag{21}$$

By using Eqs. (15) and (17) together with Eq. (21) and equation

$$P = \frac{2.0 \cdot S\sqrt{1+S}}{Fr^*} \tag{22}$$

for the Peclet number (Mols and Oliemans, 1998), we can derive that

$$R_D^+(\phi, S, Fr^*) = \frac{c_E}{\rho_l}\left(\frac{0.64}{\sqrt{1+S}} + 0.05 \cdot \frac{S}{Fr^*} \cdot \cos\phi\right) \cdot \exp\left[0.5 \cdot \frac{S\sqrt{1+S}}{Fr^*}(\cos\phi - 1)\right]. \tag{23}$$

In the derivation we have used the approximation $T_L u^*/H \approx u^*/V_{gas} \approx 0.05$. In the expression for the Peclet-number we have not included the crossing trajectories effect due to gravity, but it can easily be included. From Eq. (23) it follows that particles with a certain Stokes number S can deposit at the top if $R_D^+(\pi) > 0$, which corresponds to

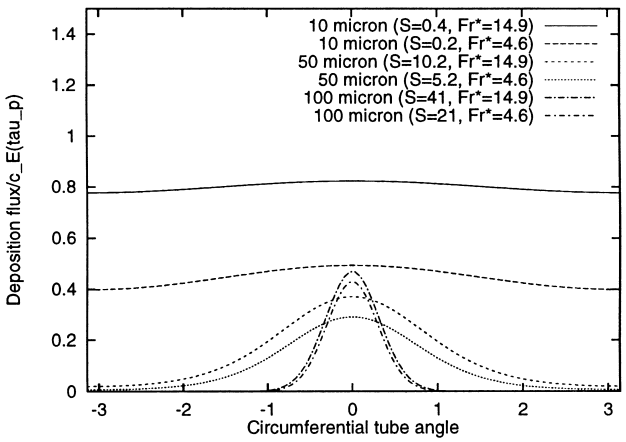

Fig. 22. Deposition flux for different S- and Fr^*-numbers as calculated in Mols and Oliemans (1998).

$$Fr^* > \frac{S\sqrt{1+S}}{12.8}. \tag{24}$$

This relation can be used as a first approximation to find out whether particles of a certain Stokes-number are able to reach the top in the tube for arbitrary conditions. From Fig. 23 one can determine for every Fr^* up to which Stokes-number particles can deposit at the top of the tube.

It is important to note that high-inertia particles experience a non-linear drag, whereas the particle relaxation time, and thus the Stokes-number S,is based on linear drag. For high inertia particles an effective particle relaxation time τ_p^{eff} can be defined as

$$\frac{1}{\tau_p^{\text{eff}}} = \frac{1}{\tau_p} C_D(Re_p)\frac{Re_p}{24}, \tag{25}$$

where C_D is the drag coefficient and Re_p the particle Reynolds number in the core area (about 80%) of the tube. Not taking into account the non-linear drag leads to a significant underprediction of the particle deposition at higher positions on the tube wall (Mols, 1999). In Eqs. (23) and (24) one should therefore for high-inertia particles use a Stokes-number based on τ_p^{eff}.

4. Concluding remarks

In this paper we have shown how a two-dimensional Turbulent Diffusion-model can be used to study dispersion and deposition of particles in a horizontal annular dispersed gas/liquid flow. The two-dimensional model is an important improvement over the one-dimensional models that have been used previously (Binder and Hanratty, 1992; Mols and Oliemans, 1998) because it makes it possible to assume any arbitrary arrangement of droplet sources along the tube wall.

A qualitative comparison was made between the two-dimensional TD-results for the particle

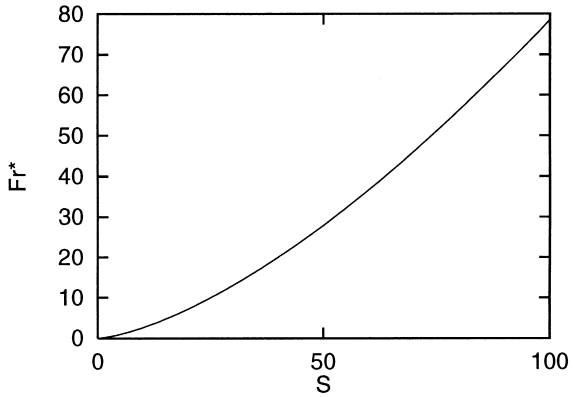

Fig. 23. Deposition at the top of the tube (for a certain Stokes-number) if Fr^* above the drawn curve. Crossing trajectories effect due to gravity has not been taken into account.

concentration and measurements of droplet fluxes and concentration found in the literature (Williams et al., 1996; Paras and Karabelas, 1991). It was concluded that the local maximum in the concentration can be explained solely by the presence of droplet sources distributed along the upper part of the tube wall as well as along the bottom part. Up till now only a secondary gas flow was held responsible for this local maximum. Although a secondary gas flow might still influence the position of the local maximum or even split a local maximum into two parts in each half of the tube-cross section, our results show that it is not a necessary condition for the appearance of the local maximum in the particle concentration.

Whereas the analytical expression was derived under the assumption that the concentration on a horizontal line in the tube is constant, the two-dimensional analysis is a straight forward, and thus more accurate method to calculate the particle concentration. For particles between 10 and 100 μm the results for the two-dimensional deposition flux show good qualitative agreement with a previously derived analytical expression (Mols and Oliemans, 1998) for the deposition flux along the tube wall. Finally we have derived how the two-dimensional deposition flux depends on the Stokes- and Froude-numbers. This expression is valid for arbitrary physical conditions.

Acknowledgements

This work has been supported by Stichting voor Fundamenteel Onderzoek der Materie (Foundation for Fundamental Research on Matter, FOM). Furthermore, the authors would like to thank Dr Mathieu Pourquié for his help in developing the numerical method to solve the two-dimensional convection/diffusion equation.

References

Azzopardi, B.J., 1997. Drops in annular two-phase flow. International Journal of Multiphase Flow 23, 1–53.

Binder, J.L., Hanratty, T.J., 1992. Use of Lagrangian methods to describe drop deposition and distribution in horizontal gas-liquid annular flows. International Journal of Multiphase Flow 18, 803–820.

Csanady, G.T., 1963. Turbulent diffusion of heavy particles in the atmosphere. Journal of the Atmospheric Sciences 20, 201–208.

Dykhno, L.A., Williams, L.R., Hanratty, T.J., 1994. Maps of mean gas velocity for stratified flows with and without atomization. International Journal of Multiphase Flow 20, 691–702.

Fukano, T., Ousaka, A., 1989. Prediction of the circumferential distribution of film thickness in horizontal and near-horizontal gas–liquid annular flows. International Journal of Multiphase Flow 15, 403–419.

Hay, K.J., Zi-Chau, Liu, Hanratty, T.J., 1996. Realtion of deposition to drop size when the rate law is nonlinear. International Journal of Multiphase Flow 22, 829–848.

Hinze, J.O., 1975. Turbulence. McGraw-Hill, New York.

Laurinat, J.E., Hanratty, T.J., Jepson, W.P., 1985. Film thickness distribution for gas–liquid annular flow in a horizontal pipe. Physico Chemical Hydrodynamicss 6, 179–195.

Lee, M.M., Hanratty, T.J., Adrian, R.J., 1989a. The interpretation of droplet deposition measurements with a diffusion model. International Journal of Multiphase Flow 15, 459–469.

Lee, M.M., Hanratty, T.J., Adrdian, R.J., 1989b. An axial viewing photographic technique to study turbulence characteristics of particles. International Journal of Multiphase Flow 15, 787–802.

Mols, B., Oliemans, R.V.A., 1998. A Turbulent Diffusion model for particle dispersion and deposition in horizontal tube flow. International Journal of Multiphase Flow 24, 55–75.

Mols, B. 1999 Particle dispersion and deposition in horizontal turbulent channel and tube flows. Ph.D. thesis, Laboratory for Aero and Hydrodynamics, Delft University of Technology, The Netherlands.

Paras, S.V., Karabelas, A.J., 1991. Droplet entrainment and deposition in horizontal annular flow. International Journal of Multiphase Flow 17, 455–468.

Pismen, L.M., Nir, A., 1978. On the motion of suspended particles in stationary homogeneous turbulence. Journal of Fluid Mechanics 84, 193–206.

Reeks, M.W., 1977. On the dispersion of small particles suspended in an isotropic turbulent field. Journal of Fluid Mechanics 83, 529–546.

Taylor, G.I., 1921. Diffusion by continuous movements. Proceedings of the London Mathematical Society 2, 196–212.

Uijttewaal, W.S.J., Oliemans, R.V.A., 1996. Particle dispersion and deposition in direct numerical and large eddy simulations of vertical pipe flows. Phys. Fluids 8, 2590–2604.

Vames, J.S., Hanratty, T.J., 1988. Turbulent dispersion of droplets for air flow in a pipe. Expts. Fluids 6, 94–104.

Williams, L.R., Dykhno, L.A., Hanratty, T.J., 1996. Droplet flux distributions and entrainment in horizontal gas–liquid flows. International Journal of Multiphase Flow 22, 1–18.